International Journal of Aerospace Engineering

Advanced Modeling Tools for Complex Turbulent Flows and its Applications

Lead Guest Editor: Nithya Subramani
Guest Editors: Yasin Şöhret and Manigandan S.

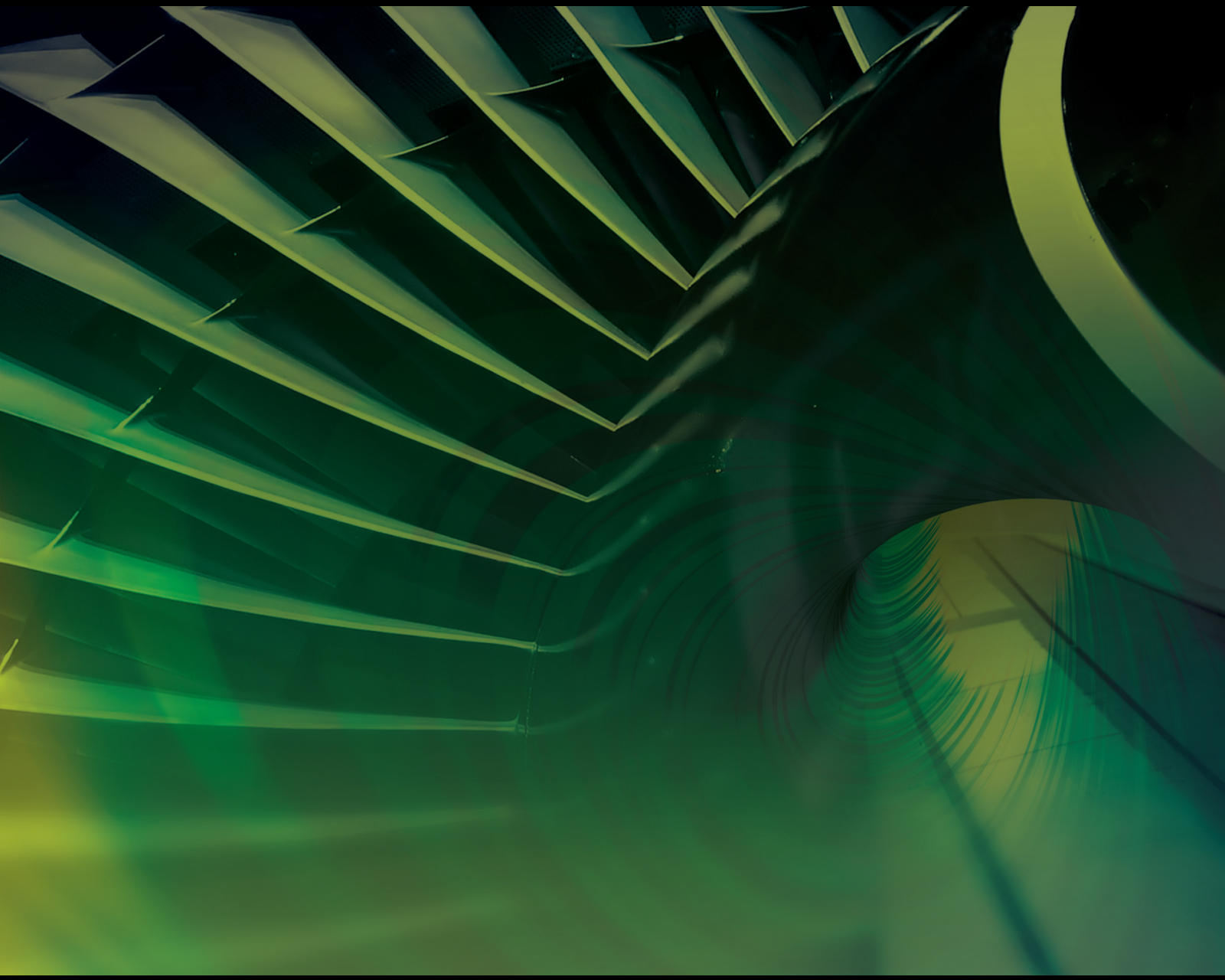

Advanced Modeling Tools for Complex Turbulent Flows and its Applications

International Journal of Aerospace Engineering

Advanced Modeling Tools for Complex Turbulent Flows and its Applications

Lead Guest Editor: Nithya Subramani
Guest Editors: Yasin Şöhret and Manigandan S.

Contents

Hindawi
International Journal of Aerospace Engineering
Volume 2023, Article ID 5813557, 18 pages
https://doi.org/10.1155/2023/5813557

Research Article

Comparative Study and Aerodynamic Analysis of Rectangular Wing Using High-Lift Systems

P. Radha Krishnan[1,2], **R. Mukesh**[2], **Inamul Hasan**[2], **P. Booma Devi**[3], **and Wubetu Amare Alebachew**[4]

[1]*Department of Aeronautical Engineering, Visvesvaraya Technological University, Belagavi, Karnataka, India*
[2]*Department of Aeronautical Engineering, ACS College of Engineering, Bangalore, Karnataka, India*
[3]*Department of Aeronautical Engineering, Sathyabama Institute of Science and Technology, Chennai, India*
[4]*Department of Mechanical Engineering, Debre Tabor University, Gondar, Amhara Region, Ethiopia*

Correspondence should be addressed to Wubetu Amare Alebachew; wubeama@dtu.edu.et

Received 22 September 2022; Revised 4 November 2022; Accepted 10 April 2023; Published 3 May 2023

Academic Editor: Nithya Subramani

High-lift systems are designed to expand the flight envelope and have a most important effect on the size of the wing, economy, and safety of many airliner configurations. Even a small increment of lift using a high-lift system can significantly impact an aircraft's profitability. The effective design of the airfoil shape with the required aerodynamic performance is still difficult. In the early days, the designs of airfoils were randomly set up and tested in the flow section, and then, the Wright brothers emerged with a cambered section. NACA has provided an appropriate airfoil definition that supports us in making airfoil designs using formulas, not randomly. This paper describes the influence of aerodynamic analysis of wing with flaps at various deflection angles. Aerodynamic variables for the aircraft wing, which is made up of the NACA airfoil 6412 model with and without flaps, have been studied at various angle of attack (AOA) (i.e., -4, -2, 0, 2, 4, 6, 8, 10, 12, and 16) and different Mach number at 0.2, 0.3, and 0.4. Also, the analysis was done for the 15000 ft altitude to check the density effects for the real-time applications. The coefficients of lift and drag are gained by examining the pressure distribution over the surface of the wing. Lift increases as the approach ascends from a low to a high angle of attack, and the most extreme lift is produced at a specific point. After that, when the angle of attack increases further, the drag component increases, so the stall occurs at that point in time. The results showed that the NACA 6412 airfoil obtained the maximum lift at 14°, and the lift value started to decrease. The CFD computations are performed in Ansys Fluent by performing hybrid mesh using ICEM-CFD. The analysis is performed for various configurations of the wing section, and the effects of flow parameters like angle of attack, altitude, and the gap distance between the main wing and slotted flap were compared to identify the better configurations.

1. Introduction

During aircraft take-off and landing, the high-lift devices have a strong influence on operating expenses and the environmental effects around the airports, such as improving fuel efficiency, payload, and noise issues. Efficient high-lift equipment with simplified construction is also expected to reduce weight, manufacturing, and maintenance costs. In aircraft wings, leading edge slats and trailing edge flaps are used as high-lift devices to obtain maximum lift coefficients during the take-off and landing of aircraft. Using aerodynamic extensions of the wing increases the effective area of the wing's footprint, thereby generating the additional lift required for an aircraft wing.

CFD is helping us to introduce innovative ideas to high-lift devices. CFD is a tool for simulating and understanding the fluid flows around objects in various conditions. CFD generally works based on resolving the governing equations of fluid mechanics, i.e., the Navier-Stokes equations, in which coupled nonlinear partial differential equation systems are solved numerically as it is rigorous to solve analytically. CFD helps engineers find near-exact approximate

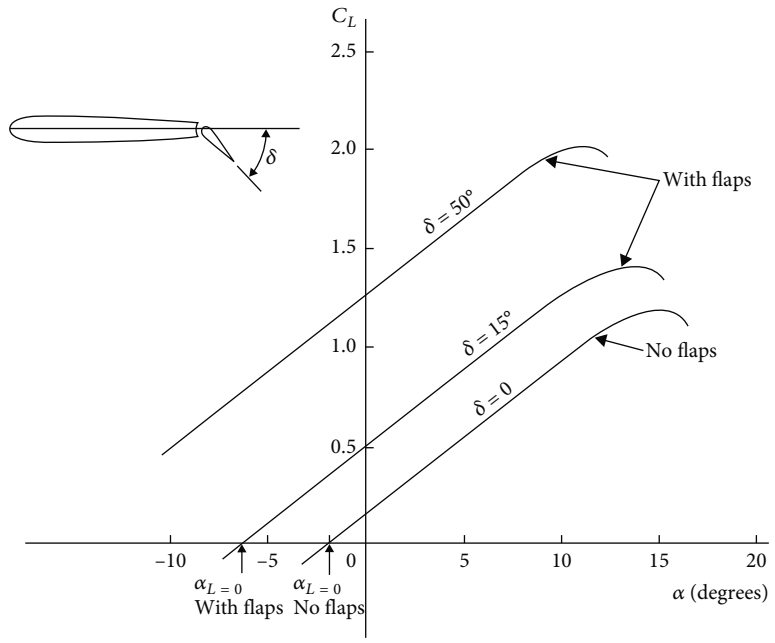

Figure 1: Effect of flap and no flap on C_L.

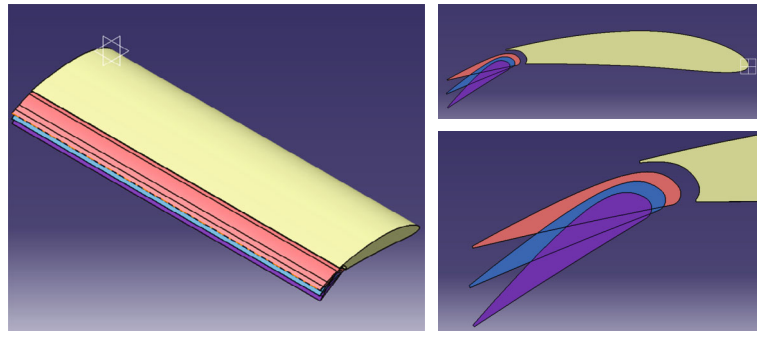

Figure 2: Wing CATIA model geometry.

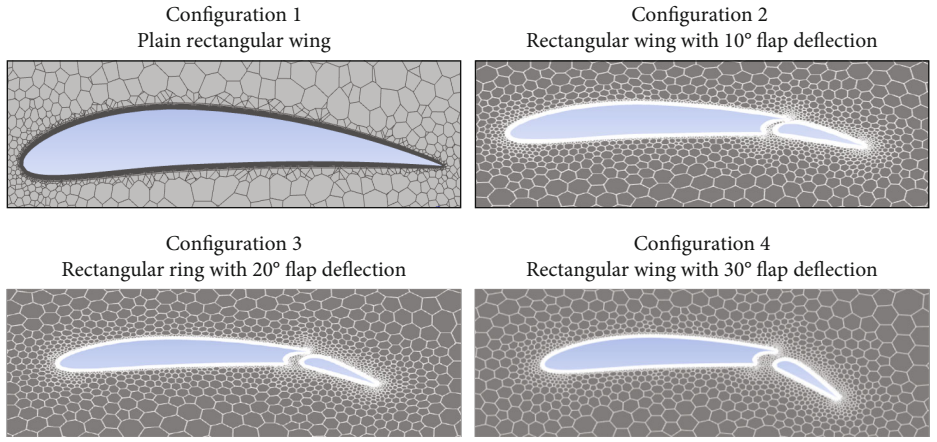

Figure 3: Wing mesh configurations.

solutions to the governing equations for various fluid flow problems. The simulation flow field analysis around the high-lift systems subjected to the methods of the solution of Reynolds-averaged Navier-Stokes (RANS) equations has seen significant progress in the last decade [1]. While designing a wing section, the accurate prediction of the aerodynamic

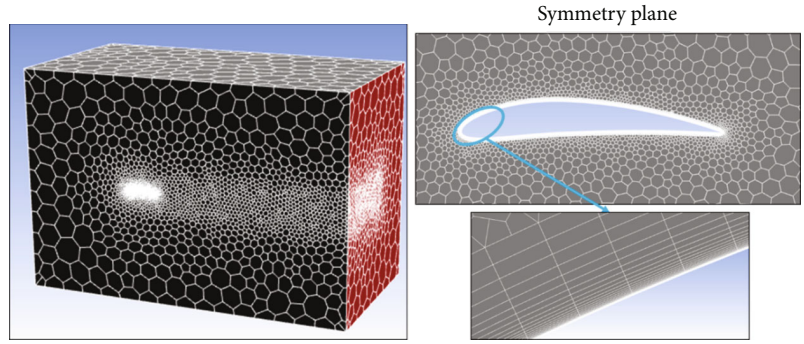

Figure 4: Polyhedral mesh conversion.

variables, such as maximum lift, maximum coefficient of lift, and L/D ratio, is very important. Identifying the actual performance of flight, including Reynolds number effects, is also an important factor. However, a high-lift device that uses trailing-edge flaps complicates the flow characteristics due to the transition in boundary layers, separation of flow, wake interaction with each element, etc. In conjunction with experiments, efforts are needed to improve CFD for high-lift systems [2].

The purpose of the flaps is to assist landing and take-off by having a higher lift with a lower stalling speed. This can be done quickly by changing the C_L of a wing, rather than AOA. A flap effectively increases the camber of an airfoil. By increasing the effective camber, a flap will shift the lift curve such that $\alpha_L = 0$ (angle of attack of zero lift) becomes more negative. The value of $C_{L\ \max}$ will also increase by a large amount. The flap effectively increases the planform area leading to an increase in $C_{L\ \max}$ by an order of 2. However, the stall angle of attack gets decreases. To overcome this, slats are used in large commercial aircraft. The effect of the downstream flap on the immediately upstream main airfoil can be modelled by placing the vortex close to the trailing edge, resulting in increased velocity on both the upper and lower surfaces. The presence of the flap, therefore, leads to increased circulation and, therefore, higher lift. Figure 1 illustrates the effect of the flap and no flap on the wing's lift coefficient (C_L).

2. Review of Literature and Theory

To attain the required flight speeds during take-off and landing is very important to fly safely for any flying vehicle. In recent studies, the increment of the coefficient of the maximum lift was the prime objective, which is intently associated with the avoidance of flow separation. Lift and drag are interrelated and depend upon the design, profile, and other factors [3, 4]. An AOA has a remarkable effect on the rise and will increase lift while also increasing drag at the factor in which drag and raise stability stall takes place [5]. In 1904, Prandtl [6] found active suction to prevent flow separation while creating the basis of boundary layer theory. Active suction technology is consequently a former technology than any passive lift boosting device. By seeing the story, we know that any passive technology used to gain a higher lift coefficient originated recently 60 years ago. Prior to 1914, Nayler et al. [7] investigated using variable camber airfoil. The leading edge slat was separately created by Lachmann [8] and Handley Page [9] in 1917. In 1927, Fowler [10] found the fundamentals for all the single and multi-slotted trailing edge devices. The droop nose designs used today on the various Airbus inboard wings came back from Bolkow in 1939 [10, 11].

Table 1: Mesh details.

First cell height	1.50E-06
Target y+	1
Reynolds number	3.20E + 06
No. of elements	1498569
No. of layers	30

Later, many evaluations came into the lift augmentation systems to improve the aerodynamic variables. Houghton et al. [12] were concerned about the trailing edge flap mechanisms, leading edge slats, and also the weight of the aircraft because of high-lift devices. When the single-slotted flap was used, the weight was increased overall by the flap panels, supports, mechanisms, actuation, and fairings. Dornheim [13] discussed two noise reduction concepts during high-lift systems' operation. There are very long chord slats (VLCS) and smart deforming droop nose concepts. These concepts show that slats' noise can possibly be reduced to 50% without affecting their performance. Rudolph [14] investigated a high-lift device by introducing a landing design having a slat and flap experimentally and arithmetically, and small-scale turbulence spots were restored from the highly dynamic free stream, and also, the intrusion of turbulence spots at the inner space of the slats was well anticipated. The maximization of the lift coefficient of airfoils provided with active control devices was analyzed by Wild [15]. And they also found that a gurney flap, one of the high-lift devices, shows the highest lift for various wing geometries from AOA 0 to 12 deg [16]. The common trailing-edge devices, leading-edge devices, and boundary control devices were the three main categories to produce high lift and avoid early flow separation in wings [17].

The small changes in the airfoil shape will help in the improvement of aerodynamic performance. Like high-lift devices, supercritical airfoils will change the airfoil shape

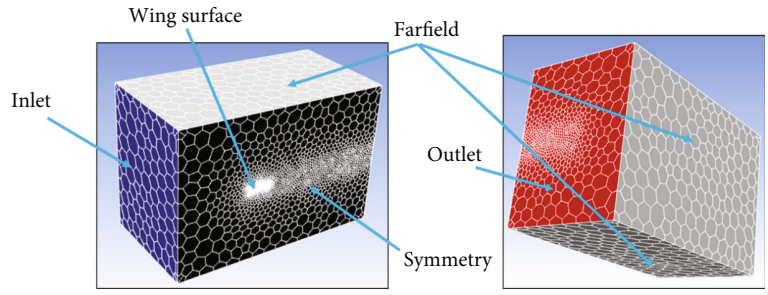

Figure 5: Boundary conditions.

and provide better aerodynamic performance and high thrust [18]. The CFD solver, mostly C-shaped or rectangle-shaped domains, realizable K-epsilon model, and K-omega turbulence model, was used for the airfoil flow analysis. And unstructured meshing can also be used for wing (3D) analysis [19]. There is a lot of evidence for the increment in the lift with respect to the high angle of attack, and flow over an airfoil separates when the velocity of the flow around the airfoil is less [20]. To do the computational analysis for the nozzles, Ansys Fluent and CFD solvers are used, and K-ε model, K-omega, and Spalart Allmaras model are used as turbulence models [21]. A lot of innovative designs alter the geometry of the airfoil used to get high lift during take-off and landing. The adaptive dropped hinge flap was one of the designs which are better than the conventional Fowler flap [22]. High-lift devices usually increase the size of the flight envelope by altering the structure of the wing section [23]. NACA 6412 airfoil series has been widely used for aerodynamic analysis from the olden days to modern days since its applications in low-speed aerodynamics [9, 24]. From this literature review, we can understand that any high-lift devices available today are following any one of these concepts. High-lift devices are almost used in many modern-day aircraft. So, introducing new concepts in high-lift devices helps to improve the aerodynamic characteristics and performance of the aircraft. And NACA 6412 airfoils can be used for low-speed aerodynamic analysis. And also, K-ε model, K-omega, and Spalart Allmaras turbulence models can be used in the CFD solver.

3. Study of Rectangular Wing Model Using NACA 6412 Airfoil

We learned the effect of fluid flow on a rectangular wing model, which was created per the NACA standards (National Advisory Committee for Aeronautics) from this work. A NACA 6412 wing profile is used in these simulations for several reasons. First, it is a classic shape that is still used for low-speed applications, e.g., gliders [9, 24, 25]. Secondly, the lift characteristics are stable at AOA up to the stall conditions, which is an advantage for UAVs. Finally, using a known aerofoil profile allows for validation of the computational fluid dynamics (CFD) of the simulation software run on Ansys Fluent. The comparison is performed based on the lift coefficient and coefficient of drag. The AOA was changed, and their effect was noticed on pressure, velocity, lift coefficient, and drag coefficient.

Table 2: Solver details and boundary conditions.

(a)

Solver details	
Solver	Pressure based-coupled
Turbulence model	SST K-omega
Fluid	Air
Flow condition	Steady state
Convergence criteria	1.00E-06

(b)

Boundary conditions	
Inlet	Velocity inlet
Outlet	Pressure outlet
Symmetry	Symmetry
Farfield	Slip wall (inviscid wall)
Wing surface	No-slip wall (viscous wall)

3.1. Geometry. The wing model is created using CATIA V5 generative shape design with a 595 mm span, and 190 mm chord NACA6412-based airfoil is shown in Figure 2. The flap chord is considered 47.5 mm, which is 25% of the main wing (typical range = 20% to 30% of the main wing). The four different configurations are created, such as plain wing, 10° flap deflections, 20° flap deflections, and 30° flap deflections. The wing-dropped hinge mechanism is used to deflect the flaps from the 0 deg position [26, 27]. The rectangular domain has been chosen for the fluid flow region.

3.2. Mesh. The hybrid mesh (prism + tetrahedral) is generated using ANSYS ICEM-CFD. The mesh has been converted into polyhedral cells in fluent without modifying prism layers, improving the mesh quality and helping to achieve better convergence. The prism layer is used to capture the boundary layer, and the density box is used to capture the wake properly [28, 29]. Reynolds number 3.20E+06 is calculated for the Mach number 0.8 so that the mesh can be used for any Mach number within 0.8. The first cell height is calculated based on this Reynolds number with a targeted y+ of 1. Mesh independence study dines to find

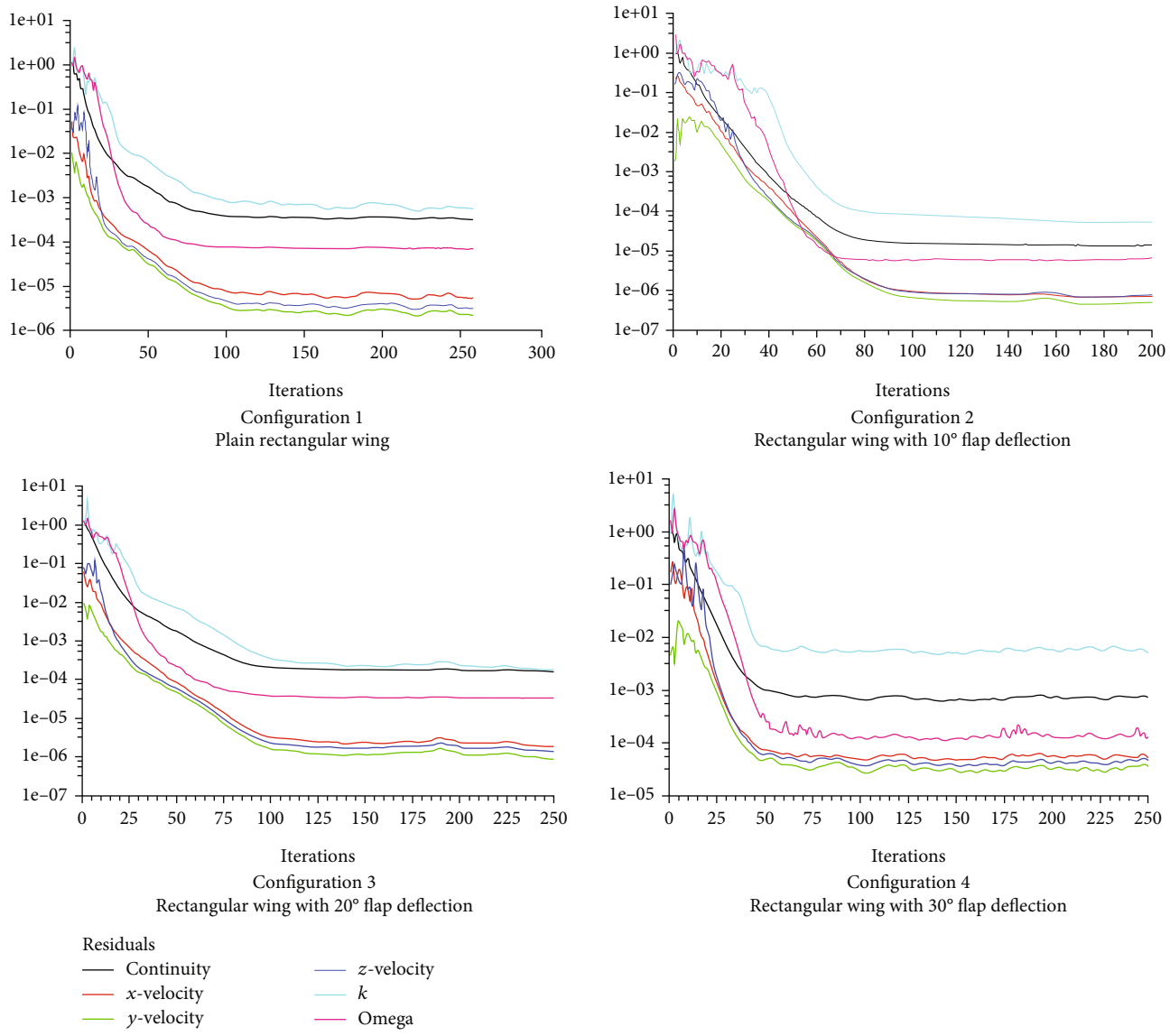

Figure 6: Typical residual plots for pressure, velocity, and turbulence parameters.

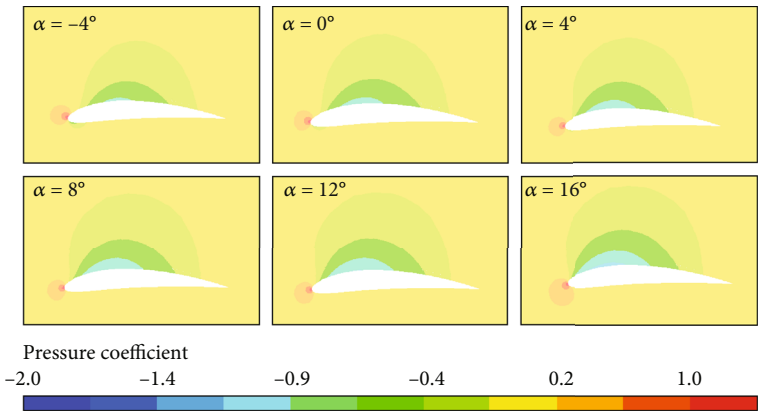

Figure 7: Pressure coefficient contour for a plain wing at Mach number 0.4.

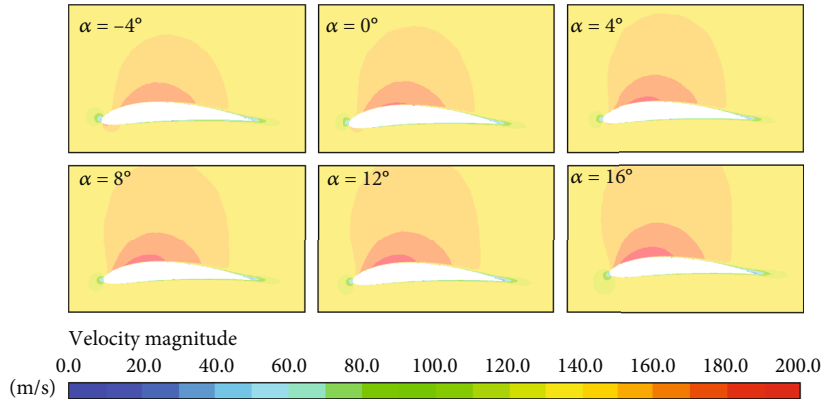

Figure 8: Velocity contour for a plain wing at Mach number 0.4.

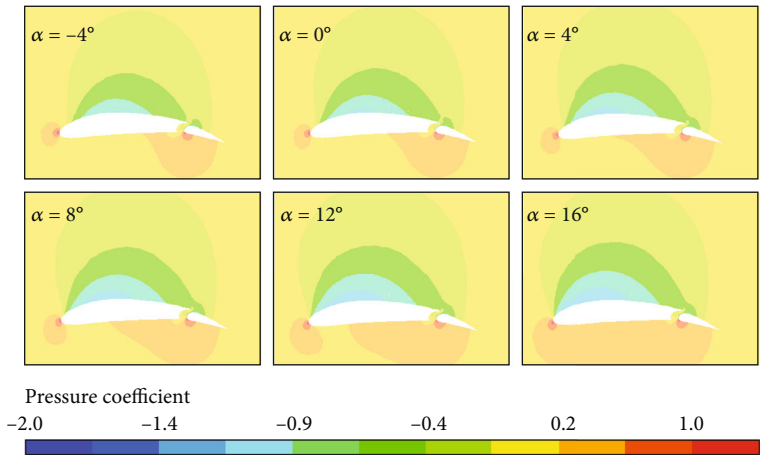

Figure 9: Pressure coefficient contour for 10-degree flap deflection at Mach number 0.4.

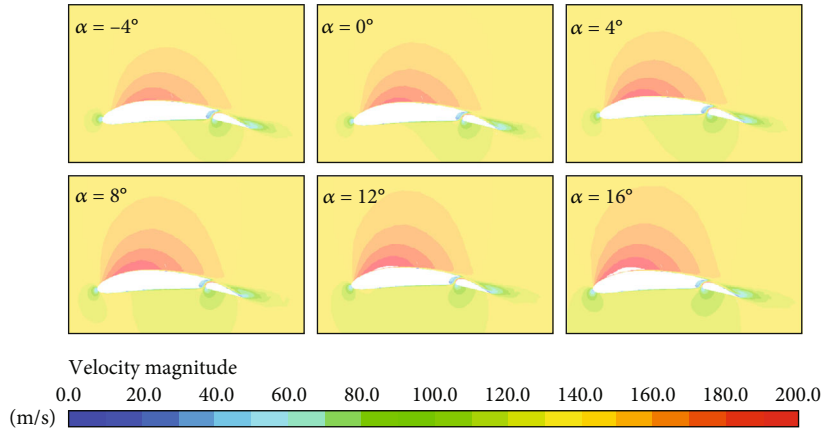

Figure 10: Velocity contour for 10-degree flap deflection at Mach number 0.4.

the optimal mesh which captures the flow physics accurately in order to avoid unnecessary refinements, which increases mesh counts and reflects in computational cost. The mesh is generated at four different configurations, such as plain rectangular wing, 10°, 20°, and 30° flap deflections cases, to be consistent with the clean wing configuration shown in Figures 3 and 4 [30, 31] and Table 1.

3.3. Computational Fluid Dynamics Simulation. Computational fluid dynamics (CFD) is used to calculate the lift distribution in the spanwise direction of the wing as the numerical approach. In CFD simulations, Ansys Fluent is used as the solver for this study. Computational fluid dynamics (CFD) has traditionally involved solving the Reynolds-averaged Navier-Stokes (RANS) equations numerically with

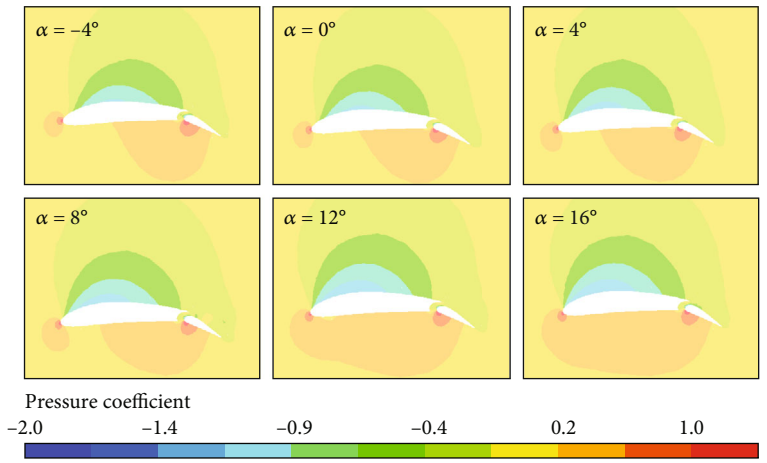

Figure 11: Pressure coefficient contour for 20-degree flap deflection at Mach number 0.4.

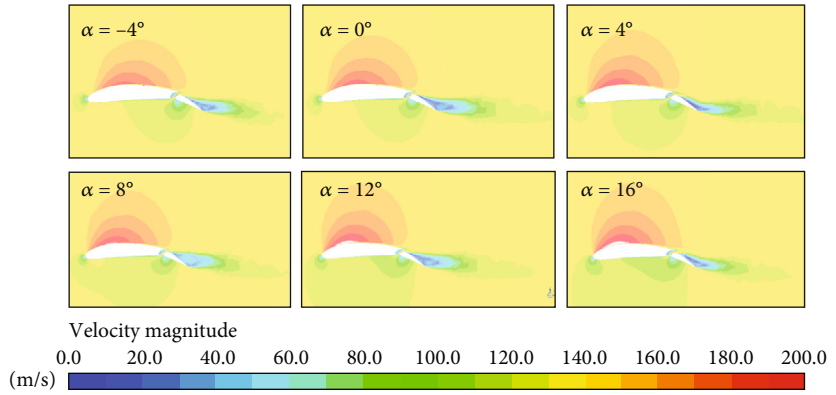

Figure 12: Velocity contour for 20-degree flap deflection at Mach number 0.4.

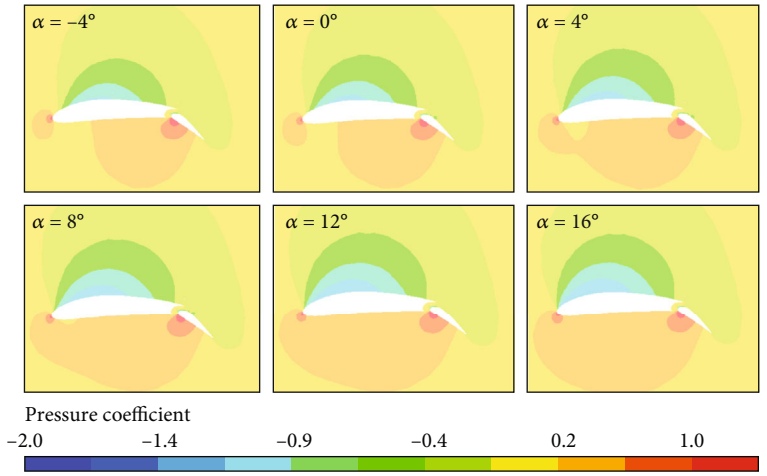

Figure 13: Pressure coefficient contour for 30-degree flap deflection at Mach number 0.4.

suitable turbulence closure models. The boundary conditions given for the analysis are shown in Figure 5. These equations are time-averaged forms of the governing continuity and momentum equations (Navier-Stokes equations (NSE)), and the turbulence model serves to close this system of mean-flow equations. The flow field was simulated using the RANS approach with the k-ω shear stress transport (SST) turbulence model and with particles tracked using a

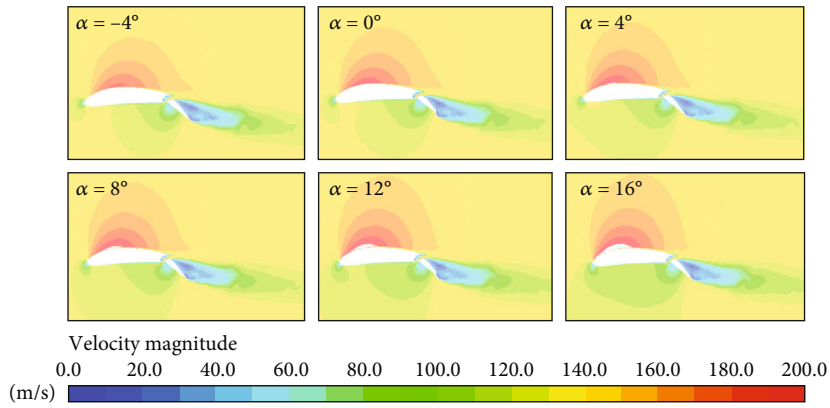

Figure 14: Velocity contour for 30-degree flap deflection at Mach number 0.4.

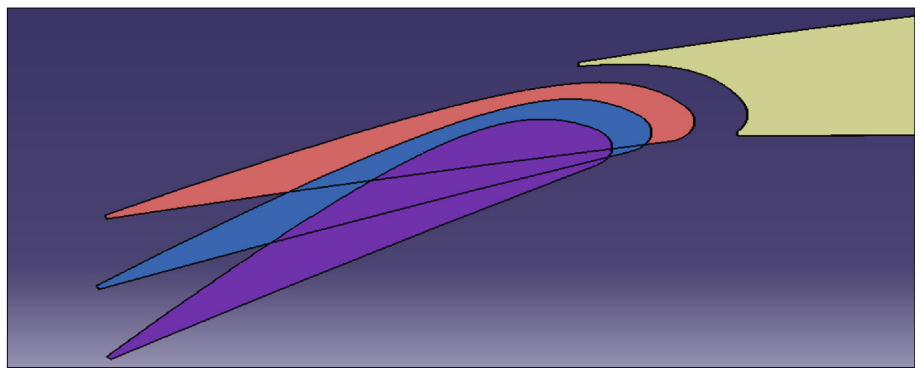

Figure 15: Flap with 10, 20, and 30 deg deflection.

Lagrangian approach. SST K-omega is known as a two-equation model [32, 33]. That means, it solves two transported partial differential equations (PDEs), which are accountable for the effects like diffusion and convection of turbulent energy in addition to the conservation equations. One of the two transported variables is turbulent kinetic energy (k), which helps to find the turbulence energy, and another is the specific turbulent dissipation rate (ω), which identifies the dissipation rate per unit of turbulent kinetic energy. Omega is also called the turbulence scale. The shear stress transport (SST) K-omega model is efficient for the better prediction of separation in the flow compared to most of the RANS models. Also, it is responsible for its better adverse pressure gradient behaviour Table 2.

3.4. SST K-Omega Turbulence Model. The SST K-omega turbulence model was introduced by Menter in 1993. It is a two-equation eddy-viscosity model. The shear stress transport (SST) model combines the two best turbulence models. Using the k-ω model in the interior parts of the boundary layer causes the model to use directly down to the wall through the viscous sublayer, so the shear stress transport (SST) k-ω model can be used as a low Reynolds turbulence model without any additional damping functions. The SST modal also changes to a k-epsilon (ε) behaviour in the free stream [20, 21, 25]. Therefore, it avoids the general k-ω problem that the model is highly sensitive to the inlet turbulence properties of the free stream. Researchers often merit the SST k-ω model high because of its good behaviour in adverse pressure gradients and separating flows [34–36].

3.5. Residual Plots. Generally, the residual plot is useful to identify the convergence nature of the iterative solution, which helps in quantifying the error in the solution of the equations as shown in Figure 6. Typical analysis in CFD includes using equations for pressure, momentum, and turbulence, and then, the solver finds the iterative solutions for these equations. The difference between these equations' successive solutions will be shown by the residual plot. In a CFD simulation, the residual measures the local imbalance of the conserved variable in each control volume [36–38]. Therefore, the wing model will have its particular residual value for every equation solved in each cell. The residual values cannot be zero in an iterative solution. However, the lesser the value of the residual, the more accurate the numerical solution is. All CFD codes will have separate procedures for normalizing the residual solutions. When judging convergence, it is best to check your code's documentation for guidance on the appropriate criterion.

3.6. CFD Results. A lot of CFD analyses were done for the various configurations of a wing with and without a flap section to find the impact of the parameters on aerodynamic

Table 3: CFD results for wing with flap gap of 7.5 mm.

Alpha	Configuration 1 plain wing		Configuration 2 flap 10° (deg)		Configuration 3 flap 20° (deg)		Configuration 4 flap 30° (deg)	
	C_L	C_D	C_L	C_D	C_L	C_D	C_L	C_D
Mach no. 0.2 @ sea level (gap 7.5 mm)								
-4°	0.4153	0.0203	0.735	0.0596	0.9055	0.1052	1.0555	0.1528
-2°	0.4484	0.0192	0.7689	0.0539	0.9371	0.1022	1.086	0.1471
0°	0.4805	0.0209	0.7948	0.0539	0.9653	0.0987	1.1149	0.143
2°	0.5115	0.0318	0.8314	0.0797	0.9938	0.1279	1.1406	0.1767
4°	0.5432	0.0489	0.8612	0.1071	1.0127	0.1654	1.1646	0.2118
6°	0.5704	0.0728	0.883	0.1355	1.0321	0.1895	1.1857	0.248
8°	0.5983	0.0974	0.9083	0.1655	1.0462	0.2263	1.2052	0.2853
10°	0.6276	0.1196	0.9311	0.1969	1.0629	0.2616	1.2227	0.3236
12°	0.6501	0.1433	0.9582	0.2405	1.0763	0.2964	1.2391	0.3629
14°	0.6662	0.1817	0.9703	0.3216	1.0709	0.3775	1.233	0.4525
16°	0.6623	0.2251	0.9317	0.4878	1.0111	0.581	1.1726	0.716
Mach no. 0.3 @ sea level (gap 7.5 mm)								
-4°	0.4213	0.0199	0.7445	0.0597	0.9194	0.1098	1.0617	0.1525
-2°	0.4545	0.0188	0.7784	0.055	0.9463	0.105	1.0926	0.1469
0°	0.4867	0.0244	0.8104	0.0539	0.9744	0.1003	1.1214	0.1427
2°	0.5178	0.0401	0.8409	0.0798	1.0051	0.1282	1.1476	0.1766
4°	0.5479	0.0576	0.8695	0.1074	1.0281	0.1613	1.1707	0.2116
6°	0.5768	0.0767	0.8963	0.1364	1.0467	0.1912	1.1924	0.248
8°	0.6048	0.0975	0.9214	0.167	1.0555	0.2233	1.212	0.2854
10°	0.632	0.1199	0.9453	0.1989	1.0723	0.2612	1.2298	0.3238
12°	0.6535	0.1448	0.9678	0.232	1.0856	0.2974	1.2421	0.3814
14°	0.669	0.1854	0.9754	0.3213	1.0819	0.388	1.239	0.4897
16°	0.6647	0.2313	0.9382	0.4977	1.0206	0.6022	1.1793	0.7519
Mach no. 0.4 @ sea level (gap 7.5 mm)								
-4°	0.4251	0.0197	0.7497	0.0596	0.9297	0.1125	1.0666	0.1524
-2°	0.4583	0.0185	0.7828	0.0543	0.9584	0.1053	1.0979	0.1468
0°	0.4896	0.0239	0.8158	0.0538	0.9826	0.0909	1.1295	0.1417
2°	0.5218	0.0398	0.8462	0.0798	1.0117	0.1263	1.1527	0.1765
4°	0.552	0.0574	0.8794	0.1024	1.0419	0.1649	1.1759	0.2116
6°	0.581	0.0767	0.9135	0.135	1.0606	0.1954	1.1974	0.2479
8°	0.609	0.0976	0.9459	0.1674	1.074	0.2257	1.217	0.2853
10°	0.6362	0.1201	0.9604	0.1995	1.0918	0.2694	1.2347	0.3238
12°	0.663	0.1441	0.9949	0.2427	1.1034	0.3117	1.2492	0.3831
14°	0.6874	0.1838	1.0021	0.3338	1.0996	0.4216	1.2431	0.4928
16°	0.6857	0.2608	0.9628	0.52	1.0374	0.6451	1.1786	0.7762

Table 4: CFD results for wing with flap gap of 15 mm.

Alpha	Mach no. 0.4 @ sea level (gap 15 mm) Configuration 1 flap 10° (deg)		Configuration 2 flap 20° (deg)		Configuration 3 flap 30° (deg)	
	C_L	C_D	C_L	C_D	C_L	C_D
-4°	0.6505	0.0561	0.7028	0.0985	0.7805	0.1364
0°	0.7067	0.0512	0.7543	0.0938	0.8283	0.1421
4°	0.7495	0.0982	0.7950	0.1426	0.8694	0.1845
8°	0.7825	0.1486	0.8387	0.1971	0.9042	0.2422
12°	0.8148	0.2322	0.8793	0.2770	0.9337	0.3234
16°	0.7716	0.5017	0.8253	0.5484	0.8775	0.6056

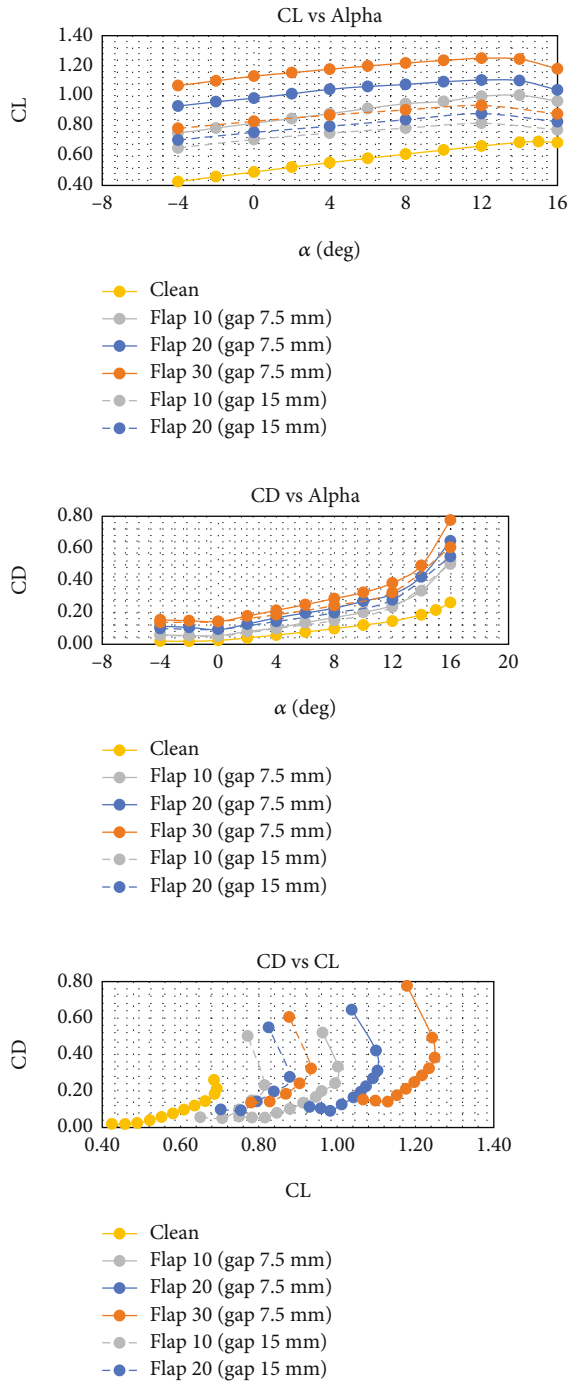

Figure 16: Comparison of gap distance between the main wing and slotted flap at Mach 0.4.

characteristics. The results were taken for all the configurations, including the case of the plain wing. The simulations have been repeated for all angles of attack from -4° to 16°. Results show that the lift coefficient is high for higher flap angles. The pressure contour and velocity contour for various angle of attack and flap deflections are obtained from CFD analysis and is given in Figures 7–14. The pressure contour shows that when the AOA changes, the pressure coefficient also varies largely. When the AOA is large, the pressure difference is also large between the upper and lower surfaces of a wing section. So, it generates a high lift, and also, it is evident that the pressure difference is more on the front portion compared to the rear portion, which tells that the lift value of an airfoil is mainly due to the front portion of the section. It can also be observed that, with an increment in Reynolds number for each angle of attack, there is an increase in the difference between the upper and lower surface pressure coefficient, thus providing the increasing lift

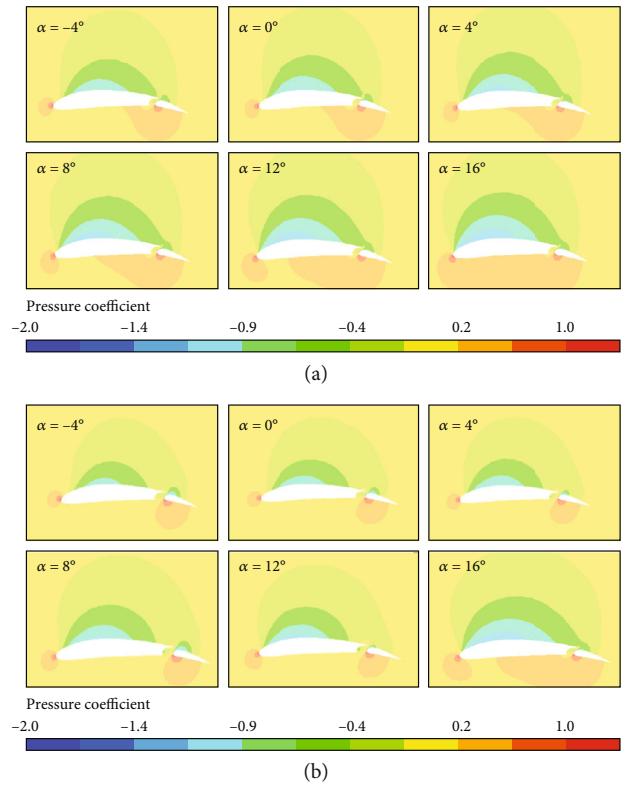

Figure 17: Comparison of gap distance between the main wing and slotted flap at Mach 0.4, 10-degree flap, and pressure coefficient contour (7.5 mm (a) and 15 mm (b)).

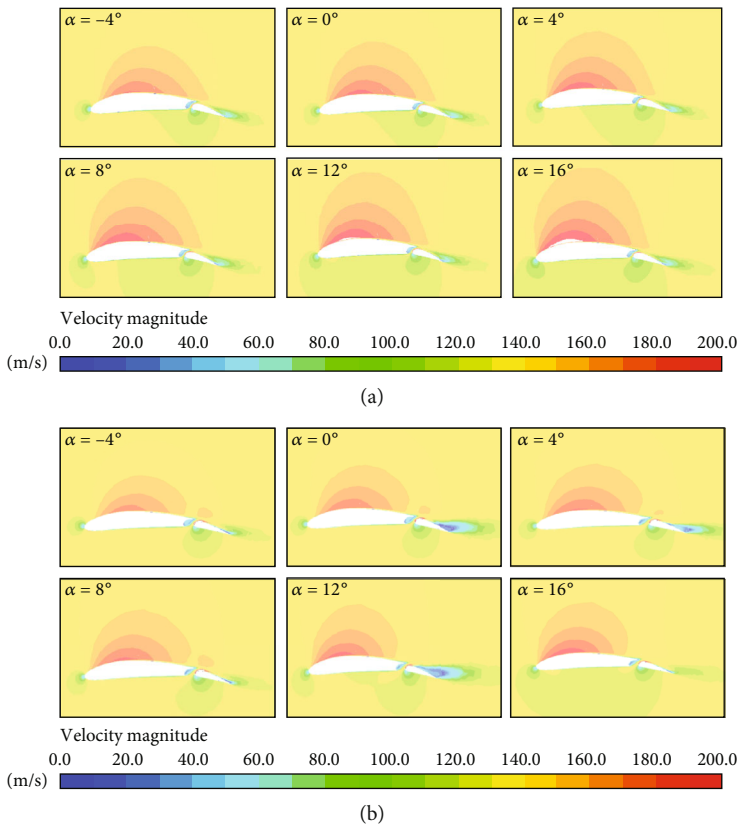

Figure 18: Comparison of gap distance between the main wing and slotted flap at Mach 0.4, 10-degree flap, and velocity contour (7.5 mm (a) and 15 mm (b)).

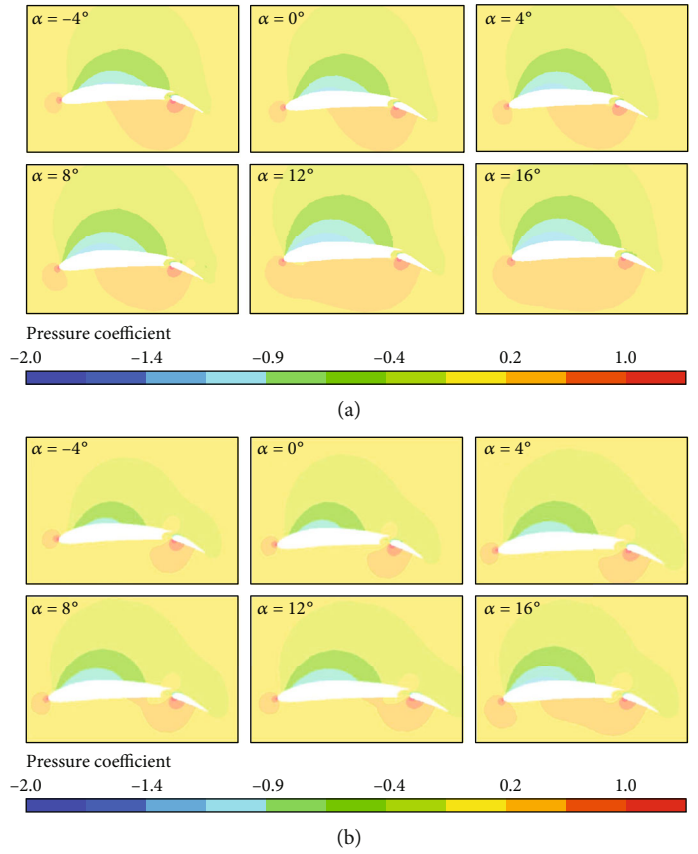

Figure 19: Comparison of gap distance between the main wing and slotted flap at Mach 0.4, 20-degree flap, and pressure coefficient contour (7.5 mm (a) and 15 mm (b)).

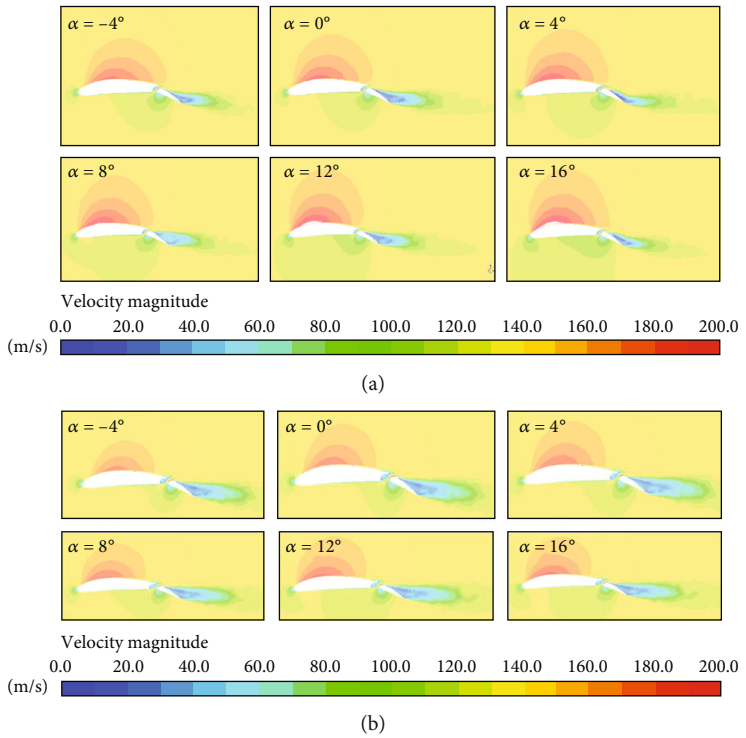

Figure 20: Comparison of gap distance between the main wing and slotted flap at Mach 0.4, 20-degree flap, and velocity contour (7.5 mm (a) and 15 mm (b)).

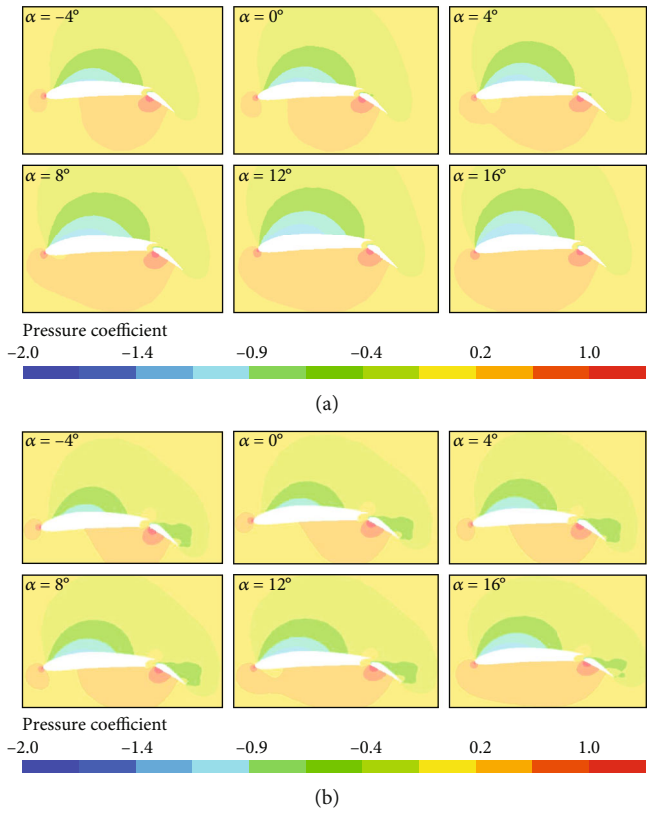

FIGURE 21: Comparison of gap distance between the main wing and slotted flap at Mach 0.4, 30-degree flap, and pressure coefficient contour (7.5 mm (a) and 15 mm (b)).

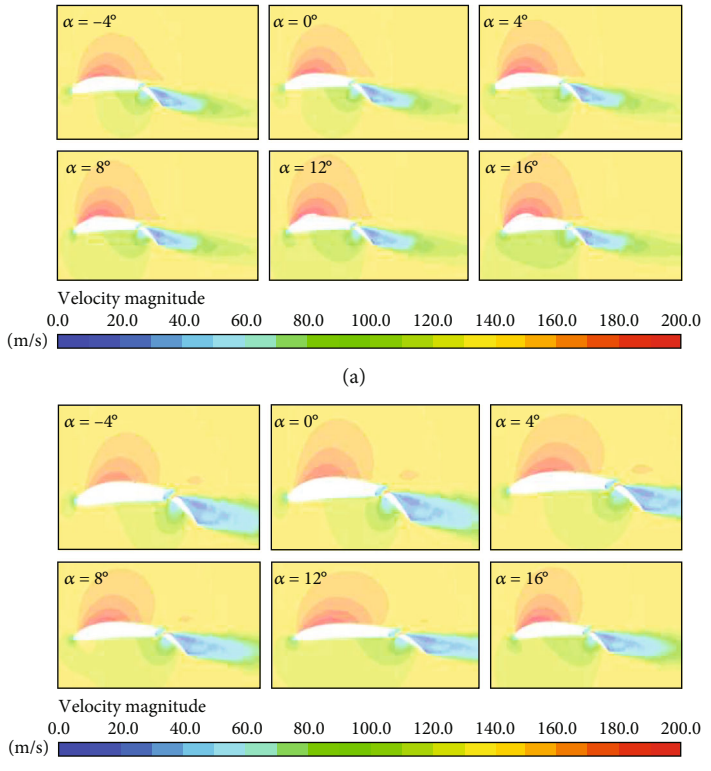

FIGURE 22: Comparison of gap distance between the main wing and slotted flap at Mach 0.4, 30-degree flap, and velocity contour (7.5 mm (a) and 15 mm (b)).

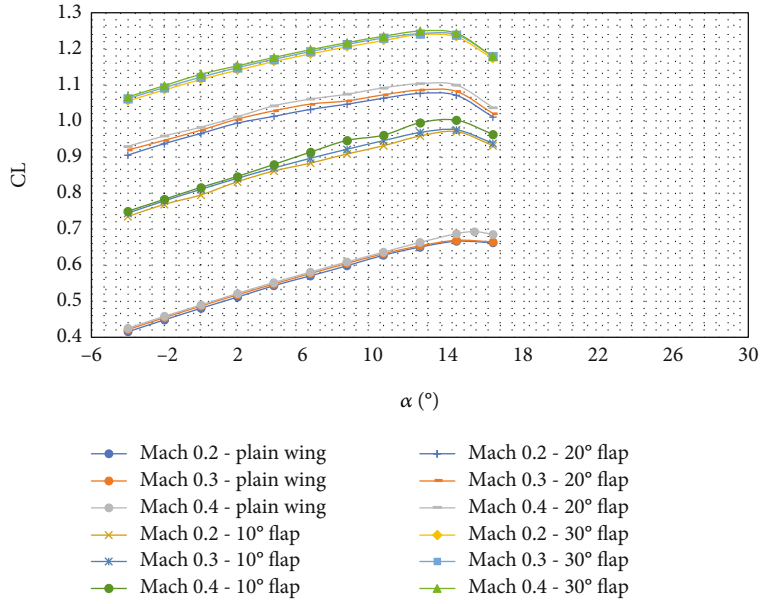

Figure 23: Effect of Mach number comparison of CL vs. alpha curves.

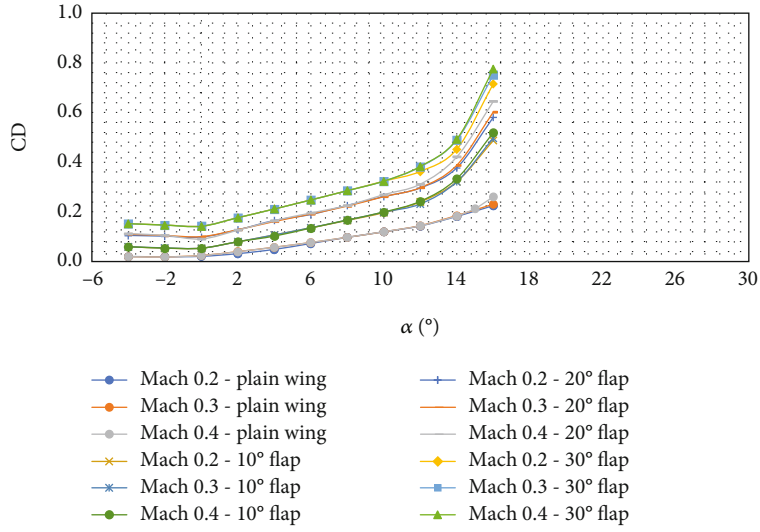

Figure 24: Effect of Mach number comparison of CD vs. alpha curves.

value. The nature of the curves is evident for the increment of lift coefficient at increasing Mach number and AOA. The study shows that the high flap angles result in a higher lift and significantly increase the drag.

4. Study of Effect of Gap Distance between the Main Wing and Slotted Flap Deflection

The main objective of this study is to find the optimal gap value between the main wing section and the slotted flap section in order to improve the aerodynamic performance of an aircraft wing. The optimal gap value between the main wing section and the slotted flap section is chosen by comparing its aerodynamic performances for two different gap values, 7.5 mm and 15 mm, respectively. The flaps with various angle of deflection are shown in Figure 15. The CFD results (Tables 3 and 4) show that the proposed lesser gap distance between the main wing and single-slotted flap shows a larger coefficient of lift than more gap distance between the main wing and single-slotted flap.

Since better results were obtained for Mach number 0.4 in the selected configuration, analysis is done with Mach number 0.4 for the gap of 15 mm. These results are tabulated below, and a comparison of values with graphs is also given below in Figure 16. The pressure contour and velocity contour for various angle of attack and flap deflections are obtained from CFD analysis and is given in Figures 17–22.

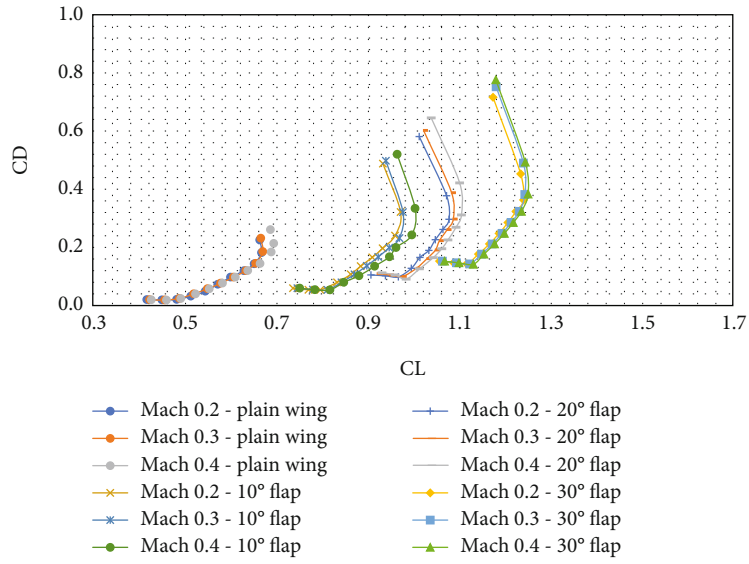

Figure 25: Effect of Mach number comparison of CL vs. CD curves.

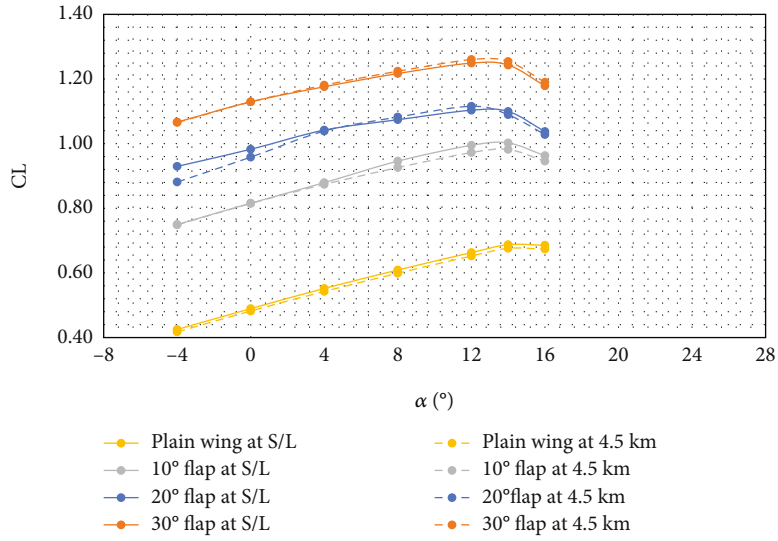

Figure 26: Effect of altitude on different configurations at Mach 0.4: CL vs. alpha curves.

5. Effect of Mach Number on Aerodynamic Variables

The objective of this work is to understand the impact of the 3D rectangular wing model at free-stream Mach numbers of 0.2, 0.3, and 0.4 at a Reynolds number of 8.62×10^5, 1.26×10^6, and 1.76×10^6. The changes in lift coefficient (C_L) with respect to the Mach number (M) can be noticed. The coefficient of lift value (C_L) is high at the increment in flap angles for any Mach number (M). Thus, it is shown in the typical curves for different values of Mach number (M). The study shows that the high flap angles result in a higher lift and considerably increase the drag. The range (R) and endurance (E) of the aircraft getting increased with decreasing in flap angles (δ). And also, for different flap angles (δ), the range (R) and endurance (E) values will come down with respect to the increment of Mach number (M). Despite that, somewhat constant endurance and range result when increasing the Mach number at larger flap angles. This broad study will facilitate a more efficient design for wing sections of aircraft and an optimized flight. The effect of Mach number with coefficient of lift and drag is shown in Figures 23–25.

6. Effect of Altitude

The purpose of this study is to understand the effect of altitude at sea level and 15000 ft (4.5 km). Lift and drag values are linearly varying with respect to the density change. The density of the air decreases when the altitude increases in the atmosphere. The graphical representation of the effect of altitude is shown in Figures 26–28. As a result, air density also changes the value of lift and drag forces proportionally.

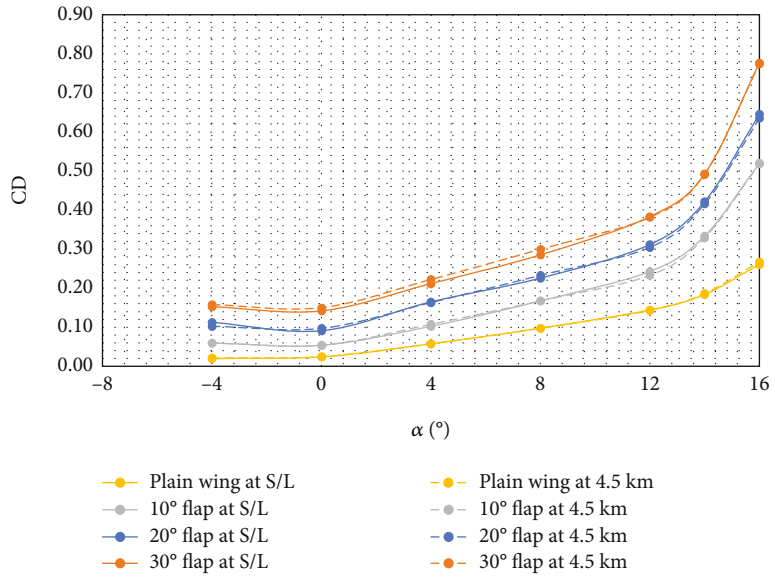

Figure 27: Effect of altitude on different configurations at Mach 0.4: CD vs. alpha curves.

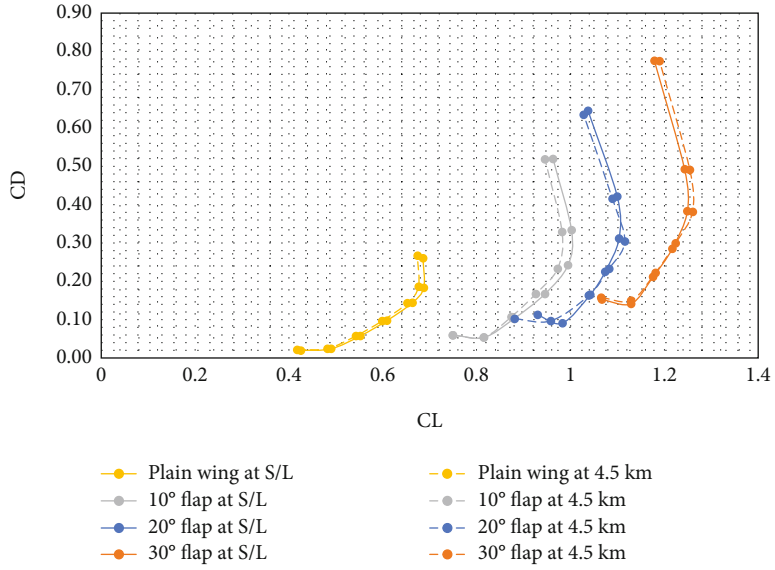

Figure 28: Effect of altitude on different configurations at Mach 0.4: CL vs. CD curves.

So, it is required for an aircraft to move at higher speeds to achieve the same lift when the density of air is low. And also, the less density of air gives less aerodynamic drag. Anyway, the lift value will be more dominant since the aerodynamic drag value is relatively small. The lift coefficient (CL) is larger for higher flap angles at sea level and 4.5 km altitude.

7. Conclusion

The following conclusions are drawn from this comparative investigation.

Aerodynamic performances for the aircraft wing model with and without flaps and having wings with NACA airfoil 6412 have been presented at various angle of attack and different Mach no. at 0.2, 0.3, and 0.4. The four different configurations have been studied, such as plain wing, 10° flap deflections, 20° flap deflection, and 30° flap deflection. The simulations have been repeated for all angles of attack from -4° to 16° (with 20 intervals). The results showed that the NACA 6412 airfoil gives a maximum lift at AOA 14°, and after that, the lift value decreases and enters into the stall mode. It is observed that the higher lift coefficient value results in higher flap angles. Also, it is noticed that the coefficient of pressure varies largely under the different angles of attack. When the AOA is large, the pressure difference between the upper and lower surfaces is greater. So, it generates a high lift. The nature of the curves is evident for the increment of lift coefficient at increasing Mach number

and AOA. The study shows that the higher flap angles obtain the higher lift and considerably increase the drag. Also, the analysis was done for the sea level and 15000 ft (4.5 km) altitude, and the results were compared. Since the density of air is low at higher altitudes, the lift value is expected to be less compared to sea-level conditions. But the results show that there is not much difference in the lift and drag values. This work has shown the possibility of numerically predicting the high lift behaviour of wing-body configurations with a flap. In the future, the optimization of different flap angles for better results and excellence could be performed. In a similar manner, flap gap distances also can be optimized to get improved results. Also, slats can be introduced at the leading edges, and their angle and gaps can be changed to identify their effects on aerodynamic characteristics.

Data Availability

The data used to support the findings of this study are available from the corresponding author upon request.

Conflicts of Interest

The authors declare that there are no conflicts of interest regarding the publication of this article.

References

[1] L. R. Rumsey and S. X. Ying, "Prediction of high lift: review of present CFD capability," *Progress in Aerospace Science*, vol. 38, no. 2, pp. 145–180, 2002.

[2] P. K. C. Rudolph, "High-lift systems on commercial subsonic airliners," NASA Contractor Report 4746, National Aeronautics and Space Administration, 1996.

[3] K. Witcher, I. R. McAndrew, and E. Vishnevskaya, "Aerodynamic analysis of low speed wing design using Taguchi L9 orthogonal array," in , Article ID 040052*017 Asia Conference on Mechanical and Aerospace Engineering (ACMAE 2017)*, vol. 151, Yokohama, Japan, 2018.

[4] R. Srinath, R. Mukesh, M. C. Poojari, I. Hasan, and W. Amare Alebachew, "Streamline effect improvement of additive manufactured airfoil utilizing dynamic stream control procedure," *Advances in Materials Science and Engineering*, vol. 2022, Article ID 1252681, 12 pages, 2022.

[5] J. Roskin, *Airplane Aerodynamics and Performance*, DARcorporation, 1997.

[6] L. Prandtl, "Über Flüssigkeitsbewegung bei sehr kleiner Reibung," in *Ludwig Prandtl Gesammelte Abhandlungen: zur angewandten Mechanik, Hydro-und Aerodynamik*, Springer, 1905.

[7] J. L. Nayler, E. W. Stedman, and W. J. Stern, "Experimental on an aerofoil having a hinged rear portion," vol. 110, Aeronautical Research Committee (ARC) Reports and Memoranda (R & M), 1914.

[8] G. Lachmann, "Unterteilte Flapchenprofile und ihre Bedeutung fur die Flugtechnik, [Ph.D. thesis]," Technische Hochschule Aachen, 1923.

[9] F. Handley Page, "Wing and Similar Member of Aircraft," 1920, US Patent 1.353.666.

[10] H. D. Fowler, "Aerofoil," 1927, US Patent 1.670.852.

[11] L. Bolkow, "Tragflugel mit Mitteln zur Veranderung der Profileigenschaft," 1939, Patentschrift Nr. 694916, Reichspatentamt.

[12] E. Houghton, P. Carpenter, S. Collicott, and D. Valentine, *Aerodynamics for Engineering Students*, Elsevier, Butterworth Hill, 7th edition, 2016.

[13] M. A. Dornheim, "Planetary flight surge faces budget realities," *Aviation Week and Space Technology*, vol. 145, no. 24, pp. 44–46, 1996.

[14] P. K. C. Rudolph, "Mechanical design of high lift systems for high aspect ratio swept wings," NASA/CR-1998-196709 National Aeronautics and Space Administration, 1998.

[15] J. Wild, "Recent research topics in high-lift aerodynamics," *CEAS Aeronautical Journal*, vol. 7, no. 3, pp. 345–355, 2016.

[16] M. Schneider, "aeroacoustic's investigation on high-lift device by using a modern hybrid RANS/LES-model," *Journal of Aeronautics & Aerospace Engineering*, vol. 6, no. 3, pp. 1–15, 2017.

[17] R. A. Gaifutdinov, "Maximization of the lift coefficient of airfoils equipped with active flow control devices," *Russian Aeronautics (Iz VUZ)*, vol. 52, no. 3, pp. 302–309, 2009.

[18] G. B. Mungekar, S. N. More, S. V. Niwate, and S. Dharmdhikari, "Effect of high-lift devices on aircraft wing," *Journal of Engineering*, vol. 2278-8719, 5 pages, 2018.

[19] A. Dal Monte, M. R. Castelli, and E. Benini, "A retrospective of high-lift device technology," *International Journal of Aerospace and Mechanical Engineering*, vol. 6, no. 11, pp. 2561–2566, 2012.

[20] I. Hasan, R. Mukesh, P. R. Krishnan, R. Srinath, and R. B. D. Prakash, "Forward flight performance analysis of supercritical airfoil in helicopter main rotor," *Intelligent Automation & Soft Computing*, vol. 33, no. 1, pp. 567–584, 2022.

[21] I. Hasan, R. Mukesh, P. Radha Krishnan, and R. Srinath, "Aerodynamic performance analysis of a supercritical airfoil in the helicopter main rotor," *Transactions of the Canadian Society for Mechanical Engineering*, vol. 46, no. 2, pp. 436–458, 2022.

[22] M. Inamul Hasan, G. Ramanan, and V. Manishankar, "Study and comparison analysis of conventional light weight UAV airfoils using XFLR analysis," *ACS Journal for Science and Engineering*, vol. 2, no. 1, pp. 1–9, 2022.

[23] V. Ramji, R. Mukesh, and I. Hasan, "Design and numerical simulation of convergent divergent nozzle," *Applied Mechanics and Materials*, vol. 852, pp. 617–624, 2016.

[24] J. I. Qiang, Z. Yufei, C. Haixin, and Y. E. Junke, "Aerodynamic optimization of a high-lift system with adaptive dropped hinge flap," *Chinese Journal of Aeronautics*, vol. 35, no. 11, pp. 191–208, 2022.

[25] S. H. Rhee, S.-E. Kim, H. Ahn, J. Oh, and H. Kim, "Analysis of a jet-controlled high-lift hydrofoil with a flap," *Ocean Engineering*, vol. 30, no. 16, pp. 2117–2136, 2003.

[26] P. R. I. S. A. C. A. R. I. U. Vasile and L. U. C. H. I. A. N. Andrei, "The aerodynamic analysis of high lift devices," in *International Conference of Scientific Paper AFASES*, pp. 83–89, Brasov, Romania, 2014.

[27] I. R. McAndrew, E. Visnehvskaya, and K. L. Witcher, "Establishing angle of attach for NACA 6412 twin-wing on take-off downwash influences on lift and drag," *International Journal of Materials, Mechanics and Manufacturing*, vol. 6, no. 4, pp. 255–259, 2018.

[28] J. G. Coder, M. D. Maughmer, and D. M. Somers, "Theoretical and experimental results for the S414, slotted, natural-

laminar-flow airfoil," in *31st AIAA Applied Aerodynamics Conference*, San Diego, CA, 2013.

[29] C. P. van Dam, "The aerodynamic design of multi-element high-lift systems for transport airplanes," *Progress in Aerospace Sciences*, vol. 38, no. 2, pp. 101–144, 2002.

[30] D. C. Eleni, T. I. Athanasios, and M. P. Dionissios, "Evaluation of the turbulence models for the simulation of the flow over a National Advisory Committee for Aeronautics (NACA) 0012 airfoil," *Journal of Mechanical Engineering Research*, vol. 4, no. 3, 2012.

[31] B. Guenther, F. Thiele, R. Petz et al., "Control of separation on the flap of a three-element high-lift configuration," in *45th AIAA Aerospace Sciences Meeting and Exhibit*, Reno, Nevada, 2007.

[32] S. Zhang, K. Srividya, I. Kakaravada et al., "A global optimization algorithm for intelligent electromechanical control system with improved filling function," *Scientific Programming*, vol. 2022, Article ID 3361027, 10 pages, 2022.

[33] C. L. Rumsey, E. M. Lee-Rausch, and R. D. Watson, "Three-dimensional effects in multi-element high lift computations," in *40th AIAA Aerospace Sciences Meeting & Exhibit*, Reno,N-V,U.S.A., 2002.

[34] R. Mukesh, K. Lingadurai, and U. Selvakumar, "Airfoil shape optimization using non-traditional optimization technique and its validation," *Journal of King Saud University-Engineering Sciences*, vol. 26, no. 2, pp. 191–197, 2014.

[35] J. H. Jo, L. P. Raj, Y. M. Lee, J. H. Lee, and R. S. Myong, "Computational Analysis of ridge iced airfoil flow field using RANS and LES," *Journal of Computational Fluids Engineering*, vol. 24, pp. 8–18, 2019.

[36] I. Hasan, R. Mukesh, P. Radha Krishnan, R. Srinath, D. P. Babu, and N. Lemma Gurmu, "Wind tunnel testing and validation of helicopter rotor blades using additive manufacturing," *Advances in Materials Science and Engineering*, vol. 2022, Article ID 4052208, 13 pages, 2022.

[37] P. T. Meredith, "Viscous phenomena affecting high-lift systems and suggestions for future CFD development," High-Lift Systems Aerodynamics, 1993.

[38] D. Zaccai, F. Bertels, and R. Vos, "Design methodology for trailing-edge high-lift mechanisms," *CEAS Aeronautical Journal*, vol. 7, no. 4, pp. 521–534, 2016.